32nd URSI GASS, Montreal, 19-26 August 2017

The Empirical Canadian High Arctic Ionospheric Model (E-CHAIM): NmF2

David R. Themens*(1), and P. Thayyil Jayachandran (1)
(1) Department of Physics, University of New Brunswick, Fredericton, NB, Canada

Abstract

It is well known that the International Reference Ionosphere (IRI) suffers reduced accuracy in its representation of monthly median ionospheric electron density at high latitudes. These inaccuracies are believed to stem from a historical lack of data from these regions. Now, roughly thirty and forty years after the development of the original URSI and CCIR foF2 maps, respectively, there exists a much larger dataset of high latitude observations of ionospheric electron density. These new measurements come in the form of new ionosonde deployments, such as those of the Canadian High Arctic Ionospheric Network, the CHAMP, GRACE, and COSMIC radio occultation missions, and the construction of the Poker Flat, Resolute, and EISCAT Incoherent Scatter Radar systems. These new datasets afford an opportunity to revise the IRI's representation of the high latitude ionosphere.

For this purpose, we here introduce the Empirical Canadian High Arctic Ionospheric Model (E-CHAIM), which incorporates all of the above datasets, as well as the older observation records, into a new climatological and storm-time representation of the high latitude ionosphere. In this presentation, we introduce the NmF2 portion of the model, focusing on both climatological and storm-time representations, and present a validation of the new model with respect to ionosonde observations from four high latitude stations. A comparison with respect to IRI performance is also presented, where we see improvements by up to 70% in the representation of peak electron density through using the new E-CHAIM model. In terms of RMS errors, the E-CHAIM model is shown to represent a near-universal improvement over the IRI, sometimes by more than 1 MHz in foF2.

1. Introduction

It is well known that the high latitude ionosphere poses significant challenges for empirical modelling through its highly dynamic nature, via coupling with the interplanetary magnetic field, and the scarcity and traditionally poor quality of data in these regions. International standards, such as the International Reference Ionosphere (IRI), have been repeatedly shown to perform poorly at high latitudes [1]. In [2], it was demonstrated that the IRI performs poorly in representing total electron content (TEC) in the Polar Cap, Auroral Oval, and Sub-Auroral regions, particularly during the equinoxes at high solar activity. These issues at high solar activity were also confirmed via Incoherent Scatter Radar (ISR) observations by [3]. [4] showed that the IRI produces significant errors in its representation of the F2 peak of the ionosphere at high latitudes, including in its representation of the topside thickness, bottomside thickness, peak electron density (NmF2), and peak height (hmF2).

Since the creation of the IRI, and similarly the NeQuick [5], electron density models, a plethora of data have become available for use in empirical modeling, namely that from new ionosonde deployments in the arctic regions and from radio occultation (RO)-based electron density inversion. These new data sources allow for the modeling of spatial scales that were not available to previous models, and satellite data, in particular, promise to improve the representation of the ionosphere in regions of sparse ground instrument coverage, such as in the arctic regions and over the oceans. It is our intention, through this work, to develop a full replacement to the use of the IRI at high latitudes. Here, we focus on the NmF2 portion of the E-CHAIM model.

2. E-CHAIM

E-CHAIM is intended as a replacement for the use of the IRI model at high latitudes. To this end, the model represents ionospheric electron density in the region above 50N geomagnetic latitude. The model is composed of several sub-models, each representing a key feature in the ionospheric electron density profile. Like the IRI, NmF2 and hmF2 are chosen as the anchor point of the profile, with all other components representing characteristics with respect to the F2 peak density and height. Each of these sub-models feature a spherical cap harmonic expansion in Altitude-Adjusted Corrected Geomagnetic (AACGM) coordinates [6], calculated at 350km altitude, for the representation of the horizontal structure of the modelled parameter, similar to those used in [7]. The order and degree of this expansion is determined experimentally, based on the amount, distribution, and quality of available data. The seasonal variability is modelled by a Fourier expansion and solar cycle variability is modelled via a function of solar F10.7 cm flux and IG ionospheric index.

3. Data

To represent the behaviour of NmF2 at high latitudes, we have gathered ionogram data from 82 ionosondes. These ionosondes include data gathered from the Canadian High Arctic Ionospheric Network (CHAIN) available at http://chain.physics.unb.ca [8], from the Global Ionospheric Radio Observatory (GIRO) available at http://giro.uml.edu/ [9], from the now decommissioned Space Physics Interactive Data Resource (SPIDR), which was available at http://spidr.ionosonde.net/spidr, from the World Data Center for Solar-Terrestrial Physics (WDC for STP, Moscow) available at http://www.wdcb.ru/stp/index.en.html, from the United Kingdom Solar System Data Center (UKSSDC) available at http://www.ukssdc.ac.uk/, and from the EISCAT Scientific Association's Dynasonde Navigator available at http://dynserv.eiscat.uit.no/. The location of these ionosondes is presented in Figure 1. For ARTIST-processed ionograms (those from GIRO), only data with a quality control index greater than 60 were included in the fitting dataset.

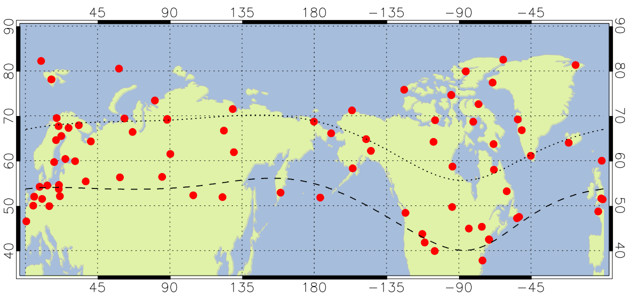

Figure 1 Plot of the global distribution of ionosondes used in the creation of the E-CHAIM.

Radio Occultation (RO) data is also gathered from the CHAMP, Gravity Recovery and Climate Experiment (GRACE), and Constellation Observing System for Meteorology, Ionosphere, and Climate (COSMIC) missions, for all occultations above 50N geomagnetic latitude. This data was gathered from the (CDAAC) data portal at http://cdaac-www.cosmic.ucar.edu/cdaac/.

For the purpose of the quiet-time model, only data corresponding to periods with Kp index less than 3.5 were included in the fitting dataset for this model. Overall, over 28 million data points are used in the fitting of the portion of the E-CHAIM model, spanning seven solar cycles.

4. Quiet-Time Model Parameterization

As mentioned in Section 2, the quiet-time NmF2 model is fitted by linear regression to a spherical cap harmonic function with Gauss coefficients tied to a Fourier expansion in day-of-year (DoY). The explicit parameterization of the model is as follows:

$$\log(NmF2) = G + \sum_{l=0}^{L}\sum_{m=0}^{\min(l,M)}\left[A_{lm}\cos\left(\frac{\pi m}{180}\lambda\right) + B_{lm}\sin\left(\frac{\pi m}{180}\lambda\right)\right]P_{lm}(\eta) \quad (1)$$

$$\eta = \cos\left((90-\varphi)\frac{\pi}{45}\right) \quad (2)$$

$$A_{lm}, B_{lm} = (\gamma_{lm}F_1 + \delta_{lm}F_2)\cdot sin^2\left(\frac{\pi\cdot DoY}{365.25}\right) + (C_{lm}F_1 + D_{lm}F_2) \quad (3)$$

$$C_{lm}, D_{lm} = \sum_{c=1}^{K}\alpha_{lm}^{c}\cos\left(\frac{2\pi c\cdot DoY}{365.25}\right) + \beta_{lm}^{c}\sin\left(\frac{2\pi c\cdot DoY}{365.25}\right) \quad (4)$$

$$G = F10.7\cdot(a_1\cos(\chi) + a_2\sin(\chi)) + \sqrt{F10.7}\cdot(a_3\cos(\chi) + a_4\sin(\chi)) + IG\cdot(a_5\cos(\chi) + a_6\sin(\chi)) + a_7F10.7^2 + a_8IG^2 \quad (5)$$

$$F_1 = F10.7_{81} \qquad F_2 = (F10.7_{81})^{(1/1.9)} \quad (6)$$

where λ is magnetic local time, φ is geomagnetic latitude, DoY is the day of year, $F10.7_{81}$ is the 81-day smoothed F10.7 solar flux gathered from the NGDC portal at ftp://ftp.ngdc.noaa.gov/STP/GEOMAGNETIC_DATA/INDICES/KP_AP, IG is the monthly ionosonde-derived IG index gathered from the UKSSDC, and χ is the solar zenith angle. α, β, γ, δ, and $a_{1\text{-}8}$ are fitting coefficients. The maximum degree (L) and order (M) for the spherical cap harmonic expansion were optimized via trial and error to be five and four, respectively. The Fourier expansion in DoY was chosen such that up to quintenial variations are represented (K = 5). Overall, these values were chosen to minimize the number of artifacts in the NmF2 representation while providing a realistic representation of the spatial gradients present in the climatological high latitude ionosphere. This proved particularly challenging when trying to realistically represent the spatial extent of auroral region enhancements in NmF2 while avoiding the creation of artifacts in regions of little data, such as the Arctic Ocean Region.

To represent diurnal variability, the model is actually composed of 24 separate models fitted to data binned in UTC. To get the NmF2 at a given point in time, linear interpolation between the models is used. Despite using 24 separate models, magnetic local time was selected as the longitudinal coordinate to reduce within-hour variability. This geomagnetic latitude-magnetic local time coordinate system was chosen due to it providing a slight improvement in performance over other coordinate systems.

The functions of F10.7 flux and the additional group of G terms, used in the above model parameterization, were selected purely experimentally via trial and error and were chosen based on maximizing the fit correlation and minimizing the fit root mean square (RMS) error.

5. NmF2 Perturbation Model

In order to match the functionality of the IRI, we have also included an ionospheric storm correction to the quiet-time model. The main driving parameters for this portion of the model were determined experimentally via trial and error and were selected as

$$G = e^{Dst\prime/300},\ e^{-ap\prime/30},\ e^{AE\prime/700} \quad (7)$$

where Dst' is the integrated hourly Dst index from the Kyoto World Data Center (WDC) for Geomagnetism, ap' is the integrated three-hour ap index from the NGDC portal, and AE' is the integrated hourly AE index gathered from the Kyoto WDC for Geomagnetism. The geomagnetic activity indices, used here, are integrated forms of the Dst, Ap, and AE indices, where integration is done in the same manner as [10] with persistence factors of 0.95, 0.75, and 0.95, respectively. Persistence factors were determined purely by trial and error using the values provided in [10] as starting points. Using a spherical cap harmonic expansion to represent horizontal variability in ionospheric storm response and the sine and cosine of the dipole tilt angle as a seasonal term, we have the following for the storm model parameterization

$$\log\left(\frac{NmF2}{NmF2}\right) = \sum_{l=0}^{L}\sum_{m=0}^{\min(l,M)}\left[A_{lm}\cos\left(\frac{\pi m}{180}\lambda\right) + B_{lm}\sin\left(\frac{\pi m}{180}\lambda\right)\right]P_{lm}(\eta) \quad (8)$$

$$A_{lm}, B_{lm} = \sum_{d=1}^{3}\left[\alpha_{lm}\sin\theta + \beta_{lm}\cos\theta + (\gamma_{lm}\sin\theta + \delta_{lm}\cos\theta)\sqrt{F10.7_{81}}\right]G_d \quad (9)$$

where λ is magnetic local time, φ is geomagnetic latitude, $F10.7_{81}$ is the 81-day smoothed F10.7 solar flux, and θ is the magnetic dipole tilt angle. α, β, γ, and δ are fitting coefficients. The maximum order and degree of the expansion was set to five and three, respectively, for this portion of the model. The reduced degree of the spherical cap expansion is a consequence of the reduction in the quality of ionosonde data during geomagnetic storm events, which tended to exaggerate noise in the storm output.

6. Validation

For the purpose of this summary paper, we shall solely examine the model validation at a single high latitude location, Resolute Canada (74.75N, 265.00E). The authors invite the reader to examine the full student paper for detailed validation results.

The validation of the quiet-time model primarily examines the model's capability to represent monthly median NmF2 and will include comparisons to the URSI foF2 maps of the IRI model. To that end, we present the monthly median NmF2 from the Resolute validation site in Figure 2.

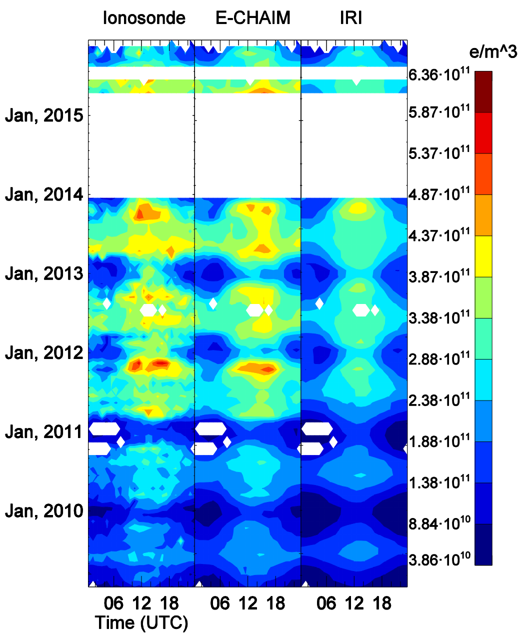

Figure 2. Ionosonde-measured (left column), E-CHAIM-modeled (middle column), and IRI-modeled (right column) NmF2 for the Resolute

Purely qualitatively, we see a significant improvement in the representation of NmF2 by the E-CHAIM model. At all stations, we see a significant improvement in the representation of equinox, daytime NmF2, particularly at high solar activity. To a lesser extent, we see a significant improvement in the representation of NmF2 during the summer daytime at solar minimum. In addition to this, the use of 81-day smoothed F10.7 flux and monthly IG index allows the E-CHAIM model to partially represent the daytime NmF2 enhancements associated with a short term increase in solar activity centered about December, 2011, which is not captured by the IRI [2].

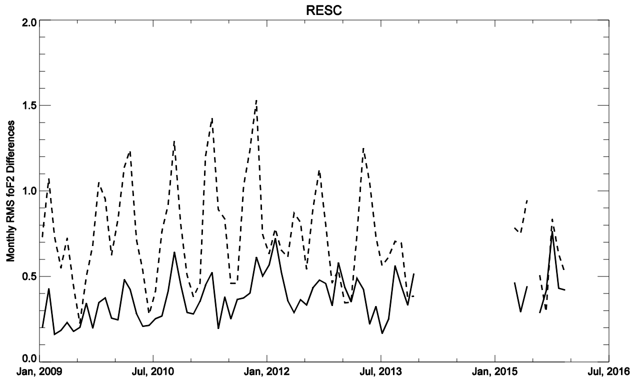

Figure 3. Monthly RMS errors in E-CHAIM (solid line) and IRI (dashed line) foF2 at the Resolute

The apparent improvement, seen in Figure 2, is reinforced when comparing the RMS errors between the models in their representation of monthly median foF2, which are presented in Figure 3. Clearly from this figure we see a dramatic improvement in the representation of foF2 by the model, particularly at solar minimum and during the equinoxes, where improvements can be by as much as 1 MHz or more.

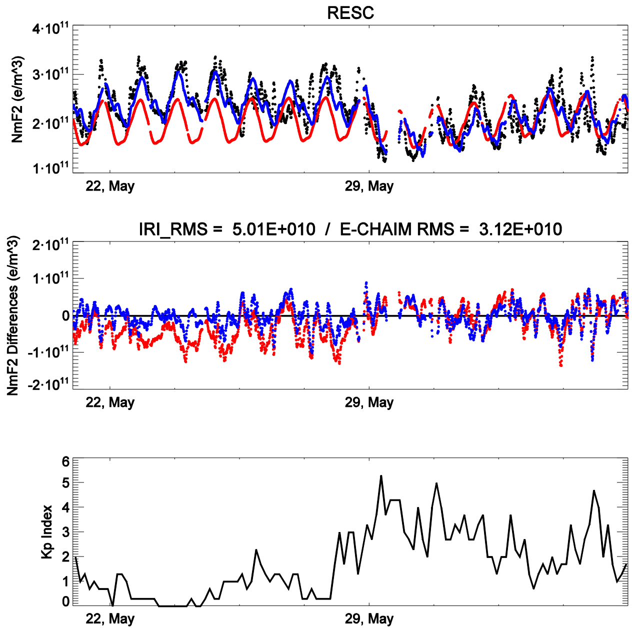

Figure 4. (Top Row) Ionosonde-measured (black), E-CHAIM modeled (blue), and IRI-modeled (red) NmF2 around the May 29th, 2010 geomagnetic storm at the Resolute. (Middle Row) Differences between observations and the E-CHAIM (blue) and IRI (red) modeled observations for the corresponding stations. (Bottom Row) Kp index for the periods presented.

To demonstrate the performance of the storm/perturbation model, we have manually scaled ionograms from Resolute and compare measured and modeled NmF2 for a moderate, and fairly long-lived, storm between May 21 and June 7, 2010, in Figure 4. We clearly see a strong negative phase response in observed NmF2 that is captured by both the E-CHAIM perturbation model and the IRI. Interestingly, the IRI also performs reasonably well during this storm, despite significant issues during the quiet periods preceding and following the storm; in fact, the IRI performs better during the storm period than during quiet periods. This, however, implies that the IRI is underestimating the storm response of the ionosphere with respect to quiet periods. In terms of improvement over the climatological E-CHAIM model, the perturbation model results in a 33% improvement at Resolute.

7. Conclusions

The work presented herein details the mathematical expressions and validation for the E-CHAIM quiet NmF2 and perturbation NmF2 models. All both models consist of a spherical cap harmonic expansion for the representation of horizontal variations, and separation into 24 separate UTC maps to account for diurnal variations. The quiet model also features a Fourier expansion in day of year, with up to quintenial terms, to represent seasonal variations and additional terms in solar zenith angle and IG index.

In the case of the quiet NmF2 model, the E-CHAIM model provides a systematic improvement over the IRI URSI maps in terms of RMS errors. Within the polar cap, we see drastic improvement over the IRI by up to 1.3MHz in critical frequency, primarily during equinox periods and at low solar activities.

To match the functionality of the IRI, the E-CHAIM model also features a storm-time adjustment model to account for ionospheric variations associated with storm periods. Comparing this storm model to that of the IRI during a prolonged Kp = 5 storm beginning on May 29, 2010, we see a significant improvement over the IRI's representation of the ionospheric response to increased geomagnetic activity. During this period, the storm parameterization constitutes an 33% improvement over the climatological model. In all cases, to our surprise, the IRI performed better during storm periods than during quiet periods.

8. Acknowledgements

Infrastructure funding for CHAIN was provided by the Canada Foundation for Innovation and the New Brunswick Innovation Foundation. CHAIN operations are conducted in collaboration with the Canadian Space Agency. Science funding is provided by the Natural Sciences and Engineering Research Council of Canada. The authors would like to thank the many ionosonde operators who provided data to this project. This paper uses ionospheric data from the USAF NEXION Digisonde network, the NEXION Program Manager is Mark Leahy. This publication makes use of data from the Qaanaaq and Nord ionosondes, owned by the U.S. Air Force Research Laboratory Space Vehicles Directorate and supported in part by the Air Force Office of Scientific Research. The authors thank Svend Erik Ascanius of the Danish Meteorological Institute and Denmark's Arctic Command for the operation of these ionosondes. This paper uses data from the Juliusruh Ionosonde which is owned by the Leibniz Institute of Atmospheric Physics Kuehlungsborn. The responsible Operations Manager is Jens Mielich. The authors are grateful to Konstantin Ratovski for the operation of these Irkutsk ionosonde.

9. References

1. Bilitza, D., and B. W. Reinisch (2008), "International Reference Ionosphere 2007: Improvements and new parameters", *Adv. Space Res.*, **42**, 599–609, doi:10.1016/j.asr.2007.07.048.
2. Themens, D.R., and P.T. Jayachandran (2016), "Solar activity variability in the IRI at high latitudes: Comparisons with GPS total electron content". *J. Geophys. Res. Space Physics*, **121**, doi:10.1002/2016JA022664.
3. Bjoland, L.M., V. Belyey, U.P. Lovhaug, and C. La Hoz (2016), "An evaluation of International Reference Ionosphere electron density in the polar cap and cusp using EISCAT Svalbard radar measurements". *Ann. Geophys.*, **34**, 751-758, doi:10.5194/angeo-34-751-2016
4. Themens, D. R., P. T. Jayachandran, M. J. Nicolls, and J. W. MacDougall (2014), "A top to bottom evaluation of IRI 2007 within the polar cap", *J. Geophys. Res. Space Physics*, **119**, 6689–6703, doi:10.1002/2014JA020052.
5. Nava, B., P. Coïsson, S.M. Radicella (2008), "A new version of the NeQuick ionosphere electron density model". *J. Atm. Sol.-Ter. Phys.*, **70**(15), 1856-1862 doi:10.1016/j.jastp.2008.01.015
6. Shepherd, S.G., (2014), "Altitude-Adjusted Corrected Geomagnetic Coordinates: Definition and Functional Approximations", *J. Geophys. Res.*, **119**, doi:10.1002/2014JA020264
7. Yamazaki, Y., M.J. Kosch, and E.K. Sutton (2015), "A model of high-latitude thermospheric density". *J. Geophys. Res. Space Phys.*, **120**, doi:10.1002/2015JA021371
8. Jayachandran, P. T., R. B. Langley, J. W. MacDougall, S. C. Mushini, D. Pokhotelov, A. M. Hamza, I. R. Mann, D. K. Milling, Z. C. Kale, R. Chadwick, T. Kelly, D. W. Danskin, and C. S. Carranoet (2009), "Canadian High Arctic Ionospheric Network (CHAIN)", *Radio Sci.*, **44**, RS0A03, doi: 10.1029/2008RS004046.
9. Reinisch, B. W., and I. A. Galkin (2011), "Global ionospheric radio observatory (GIRO)", *Earth, Planets, and Space*, **63**, 377-381, doi:10.5047/eps.2011.03.001
10. Wu, J., and P.J. Wilkinson (1995). "Time-weighted magnetic indices as predictors of ionospheric behavior", *J. Atm. Sol.-Ter. Phys.*, **57**(14), 1763-1770